XVIIIth symposium
Vibrations, Chocs et Bruit* & ASTELAB
*VISHNO (VIbrations, SHocks & NOise)
July 3, 4 and 5, 2012
Centre de recherche EDF
de Clamart

Vibrations, Shocks and Noise

Low-order Local Modelling of Structural Nonlinearities

J.P. Noël*, G. Kerschen

Space Structures and Systems Lab (S3L)
Department of Aerospace and Mechanical Engineering
University of Liège
1 Chemin des chevreuils (B52/3), 4000 Liège, Belgium

Abstract

The present paper addresses the problem of characterising structural nonlinearities in view of system identification. A low-order local modelling strategy is proposed and encapsulated in a recently-introduced frequency-domain nonlinear subspace method for the estimation of model parameters. The complete methodology is first demonstrated using two academic examples, namely a Duffing oscillator and a five-degree-of-freedom system comprising two nonlinearities. The identification of an experimental beam involving nonlinear geometrical behaviour is finally addressed.

Keywords: Nonlinear system identification ; nonlinearity characterisation ; low-order piecewise polynomials ; numerical and experimental data.

1. Introduction

The nonlinear identification process in structural dynamics can be viewed as the succession of three steps, namely detection, characterisation and parameter estimation. Once nonlinear behaviour is detected, a nonlinear system is said to be characterised after the location, type and functional form of all the nonlinearities throughout the system are determined. The parameters of the selected model are then estimated using, *e.g.*, linear least-squares fitting or nonlinear optimisation algorithms depending upon the method considered. As stressed in the survey paper [1], an accurate characterisation of the nonlinear elastic and dissipative behaviour of the structure is of utmost importance. Today, this task remains challenging because nonlinearity may be caused by many different mechanisms and may result in plethora of dynamic phenomena. In the technical literature, the most standard practice is to resort to high-order global polynomial expansion (see for instance [2] concerning the use of Chebyshev polynomials). The principle of polynomial expansion is to approximate the restoring force by a unique polynomial of some degree in displacement and velocity. However, in many circumstances, *e.g.* non-smooth or non-integer exponent-type nonlinearities, this approach may not be effective.

In this context, the present paper introduces the use of a low-order spline-based approximation strategy, which avoids the need for having *a priori* information about the physical structure. This piecewise-polynomial modelling is herein coupled with a recently-introduced frequency-domain subspace-based method for the estimation of model parameters, referred to as the Frequency-domain Nonlinear Subspace Identification (FNSI) method. Section 2 states the identification problem treated in this work and formulates linear and third-order spline approximations in the case of elastic nonlinearity. Section 3 gives an introduction to the different steps of the FNSI technique and outlines its major assets. The complete methodology is then demonstrated using two academic examples in Section 4, namely a Duffing oscillator and a five-degree-of-freedom system comprising two nonlinearities. The identification of an experimental beam involving nonlinear geometrical behaviour is finally addressed in Section 5.

* Corresponding author. Tel.: +32-4-366-48-54. E-mail address: JP.Noel@ulg.ac.be

2. Problem statement and proposed modelling of nonlinearities

The present paper addresses the identification of nonlinear mechanical systems whose nonlinearities are supposed to be localised and for which there exists an underlying linear regime of vibration. The amplitude, the direction and the frequency content of the excitation determine in which regime the structure behaves. The vibrations of such nonlinear systems are governed by the time-continuous model

$$M\,\ddot{q}(t) + C\,\dot{q}(t) + K\,q(t) + f(q(t),\dot{q}(t)) = p(t) \tag{1}$$

where M, C, $K \in \mathbb{R}^{r\times r}$ are the mass, damping and stiffness matrices, respectively, $q(t)$ and $p(t) \in \mathbb{R}^r$ are the generalised displacement and force vectors, $f(t) \in \mathbb{R}^r$ is the nonlinear restoring force vector and r is the number of degrees of freedom (DOFs) of the structure obtained after spatial discretisation. In the frequency domain, this model becomes

$$B(\omega)\,Q(\omega) + F(\omega) = P(\omega) \tag{2}$$

where $Q(\omega)$, $F(\omega)$ and $P(\omega)$ are the Fourier transforms of $q(t)$, $f(t)$ and $p(t)$, respectively, and $B(\omega) = (-\omega^2 M + i\omega C + K)$ is the linear dynamic stiffness matrix.

The effect of the j lumped nonlinearities are modelled using the summation

$$\sum_{s=1}^{j} \mu_s\, b_s\, g_s\big(q(t),\dot{q}(t)\big). \tag{3}$$

Each term contains information about the strength of the nonlinearity μ_s, its location $b_s \in \mathbb{R}^r$ and its functional form g_s. In this work, we propose to consider low-order piecewise polynomials as nonlinear basis functions g_s. For the sake of simplicity, we restrict our scope to elastic nonlinearities $g_s\big(q(t)\big)$.

Let q be divided into M segments with arbitrary length defined by their bounds denoted a^k, where k varies from 1 to $M+1$. The samples of q belonging to the k^{th} segments (bounded by a^k and a^{k+1}) are noted q^k. Over each segment, we introduce the normalised displacement n^k, defined in the unit interval $(0,1)$ as

$$n^k = \frac{q^k - a^k}{a^{k+1} - a^k}. \tag{4}$$

A first-order piecewise approximation of g_s is then given by

$$\begin{aligned} g_s^k &= \left(\frac{b^{k+1} - b^k}{a^{k+1} - a^k}\right)(q^k - a^k) + b^k \\ &= (b^{k+1} - b^k)\,n^k + b^k \end{aligned} \tag{5}$$

where the ordinates b^k of the segment end points a^k are the sought coefficients in the nonlinear identification problem. It is worth pointing out that this writing enforces zero-order continuity between adjacent segments. From Equation (5) evaluated in $k-1$ and k, each coefficient b^k is found to be associated with the basis function

$$n^{k-1} + (1 - n^k) \tag{6}$$

which will be considered as an input term of the FNSI algorithm, as developed in Section 3.1. Though being simple, the former linear approximation cannot offer first-order continuity. This is achieved using the third-order piecewise approximation of g_s

$$g_s^k = b^k\,h^{1,k} + s^k\,h^{2,k}\,(a^{k+1} - a^k) + b^{k+1}\,h^{3,k} + s^{k+1}\,h^{4,k}\,(a^{k+1} - a^k) \tag{7}$$

where s^k is the slope of the nonlinear restoring force curve in $q = a^k$ and $h^{1,k}$, $h^{2,k}$, $h^{3,k}$ and $h^{4,k}$ are known as the Hermite polynomials, defined as

$$\begin{aligned} h^{1,k} &= 2(n^k)^3 - 3(n^k)^2 + 1 \\ h^{2,k} &= (n^k)^3 - 2(n^k)^2 + n^k \\ h^{3,k} &= -2(n^k)^3 + 3(n^k)^2 \\ h^{4,k} &= (n^k)^3 - (n^k)^2. \end{aligned} \tag{8}$$

Therefore, the ordinate b^k and the slope s^k are found to be associated with the basis functions

$$h^{1,k} + h^{3,k-1} \tag{9}$$

and

$$h^{2,k}(a^{k+1} - a^k) + h^{4,k-1}(a^k - a^{k-1}), \tag{10}$$

respectively.

3. Frequency-domain nonlinear subspace identification methodology

The FNSI technique is a five-step methodology. They will be successively described in the present section and summarised in a flowchart.

3.1. Step 1: Joint collection of excitations and nonlinearities as input data

An appealing approach for interpreting the dynamics governed by Equation (1) consists in moving the nonlinear term to the right-hand side and viewing nonlinear forces as external forces applied to the underlying linear structure:

$$M\,\ddot{q}(t) + C\,\dot{q}(t) + K\,q(t) = p(t) - f(t). \tag{11}$$

Doing so, the internal forces that are nonlinear functions of the outputs act as a feedback to the linear open-loop system. This peculiar feedback form allows the transition to an equivalent linear system identification problem [3]. Moreover, we opt for a discrete-time state-space modelling for numerical conditioning reasons [4]. Thus, our objective is to fit to observations a state-space model of the form

$$\begin{cases} x(t+1) = A\,x(t) + B\,u(y,t) \\ y(t) = C\,x(t) + D\,u(y,t) \end{cases} \tag{12}$$

where $A \in \mathbb{R}^{n\times n}$ prescribes the linear dynamics of the system, $B \in \mathbb{R}^{n\times m}$ contains the parameters b^k (and possibly s^k) that are eventually sought, $C \in \mathbb{R}^{l\times n}$ is the output matrix, $D \in \mathbb{R}^{l\times m}$ is the direct feed-through matrix, $u(y,t) \in \mathbb{R}^m$ concatenates the excitation signals *and* the low-order piecewise basis functions, $x(t) = (q\ \dot{q})^T \in \mathbb{R}^n$ is the state vector, $y(t) \in \mathbb{R}^l$ is the measured output vector and $n = 2\,r$.

3.2. Step 2: Formulation in the frequency domain

Tackling system identification problems in the frequency domain is an attractive and versatile alternative [5], *e.g.* because experimental data are often recorded as Frequency Response Functions (FRFs), power spectral densities or simply spectra. It is also worth pointing out that frequency-domain subspace algorithms proved successful in linear identification problems [6]. This motivates us to approach nonlinear mechanical structures by using subspace methods formulated in the frequency domain. To this end, Equations (12) are recast by use of the Discrete Fourier Transform (DFT).

The DFT $V(k)$ of a time signal $v(t)$ is given by (provided that $v(t)$ is periodic and observed over an integer number of periods in steady-state conditions)

$$V(k) = \frac{1}{\sqrt{R}} \sum_{t=0}^{R-1} v(t) e^{-j\,2\pi\,k\,t/R} \tag{13}$$

where R is the number of recorded time samples of v, k is the frequency line and j is the imaginary unit. Equations (12) thus write

$$\begin{cases} z_k\,X(k) = A\,X(k) + B\,U(k) \\ Y(k) = C\,X(k) + D\,U(k) \end{cases} \tag{14}$$

where $X(k)$, $U(k)$ and $Y(k)$ are the DFTs of $x(t)$, $u(y,t)$ and $y(t)$, respectively.

Equations (14) are commonly recast into matrix form in the subspace literature (for more details, we refer the reader to [4]):

$$Y_i = \Gamma_i \, X + H_i \, U_i \tag{15}$$

where Y_i, U_i and X gather entire spectra, Γ_i and H_i contain the state matrices only and the index i indicates the number of block rows of a matrix. The extended observability matrix Γ_i plays a major role in subspace theory as underlined in *Step 3* and Equation (15) will be exploited in *Step 4*.

3.3. Step 3: Estimation of Γ_i, A and C

The purpose of subspace algorithms is the computation of the extended observability matrix using geometrical projections of input-output data. This computation starts with the cancellation of the input term in Equation (15) by means of orthogonal projection [7]. Secondly, estimates of Γ_i and of the system order n are obtained through a truncated singular value decomposition. To detail this procedure (see [6]) and to examine its theoretical foundations (see [3]) are beyond the scope of this paper.

From the knowledge of Γ_i, further stages then consist in finding the best way to estimate the state matrices. In frequency-domain algorithms, A and C are efficiently computed from the so-called shift property of Γ_i [8]. We also follow this way in our methodology. An effective computation of B and D is more delicate and a robust numerical scheme is proposed in Section 3.4.

3.4. Step 4: Estimation of B and D

The core of the demonstration is inspired by [7] although several major adaptations are proposed to meet our frequency-domain formulation. First, we substitute in Equations (14) the state spectrum X and its frequency derivative $X\,\zeta$ by using the output-state-input Equation (15) and its transformed version

$$Y_i \, \zeta = \Gamma_i \, X \, \zeta + H_i \, U_i \, \zeta \tag{16}$$

where $\zeta = \mathrm{diag}[z_1 \; z_2 \; ... \; z_N]$ considering N (non-necessarily equidistant) frequency lines. We secondly observe that

$$\begin{cases} Y_i = \underline{Y_{i+1}} \\ U_i = \underline{U_{i+1}} \end{cases} \text{ and } \begin{cases} Y_i \, \zeta = \overline{Y_{i+1}} \\ U_i \, \zeta = \overline{U_{i+1}} \end{cases} \tag{17}$$

where the operators $\underline{Z}$ and $\overline{Z}$ remove from their argument Z the last and first block rows, respectively. These shift properties can be realised by simply considering the data matrix structure presented, for instance, in [4]. We consequently eliminate X and $X\,\zeta$ by the relations

$$\begin{cases} X = \Gamma_i^{\dagger} (\underline{Y_{i+1}} - H_i \, \underline{U_{i+1}}) \\ X \, \zeta = \Gamma_i^{\dagger} (\overline{Y_{i+1}} - H_i \, \overline{U_{i+1}}) \end{cases} \tag{18}$$

where † denotes the inverse of a non-square matrix. For the sake of convenience, identity and zero matrices are preferred to under- and overline operators as

$$\begin{cases} X = \Gamma_i^{\dagger} \left(\mathrm{I}^{[li]} \mid 0^{[li \times l]} \right) Y_{i+1} - \Gamma_i^{\dagger} H_i \left(\mathrm{I}^{[mi]} \mid 0^{[mi \times m]} \right) U_{i+1} \\ X \, \zeta = \Gamma_i^{\dagger} \left(0^{[li \times l]} \mid \mathrm{I}^{[li]} \right) Y_{i+1} - \Gamma_i^{\dagger} H_i \left(0^{[mi \times m]} \mid \mathrm{I}^{[mi]} \right) U_{i+1} \, . \end{cases} \tag{19}$$

Some simple manipulations lead to the final writing of the state-space equations

$$\left(\frac{\Gamma_i^{\dagger} \left(0^{[li \times l]} \mid \mathrm{I}^{[li]} \right) Y_{i+1}}{Y} \right) = \left(\frac{A}{C} \right) \Gamma_i^{\dagger} \left(\mathrm{I}^{[li]} \mid 0^{[li \times l]} \right) Y_{i+1} + \mathcal{K} \, U_{i+1} \tag{20}$$

where

$$\mathcal{K} = \left(\frac{\left(B \mid \Gamma_i^{\dagger} H_i \right) - \left(\mathrm{A} \, \Gamma_i^{\dagger} H_i \mid 0^{[mi \times m]} \right)}{\left(D \mid 0^{[l \times mi]} \right) - \left(C \, \Gamma_i^{\dagger} H_i \mid 0^{[mi \times m]} \right)} \right). \tag{21}$$

Two features of Equation (20) must be emphasised. First, the matrix $\mathcal{K}$, which exclusively contains the state matrices, is the single unknown of the problem. The new quantities $\mathcal{P}$ and $\mathcal{Q}$ are thus introduced as

$$\mathcal{P} = \left(\frac{\Gamma_i^{\dagger} \left(0^{[li \times l]} \mid \mathrm{I}^{[li]} \right) Y_{i+1}}{Y} \right) - \left(\frac{A}{C} \right) \Gamma_i^{\dagger} \left(\mathrm{I}^{[li]} \mid 0^{[li \times l]} \right) Y_{i+1} \tag{22}$$

and

$$Q = U_{i+1} \,. \tag{23}$$

Therefore, B and D can be computed as the solution of the least-squares problem

$$B, D = \arg \min_{B,D} \| \mathcal{P} - \mathcal{K}(B, D) \mathcal{Q} \|^2 \,. \tag{24}$$

Secondly, $\mathcal{K}$ is linear in B and D. This causes the aforementioned optimisation problem to be convex. Despite this appealing property, we pursue another way to solve the problem. Indeed, for efficiency purposes, Equation (24) is eventually rewritten as an explicit linear combination of B and D and solved in least-squares sense.

3.5. Step 5: Conversion of the system model into the nonlinearity model

The final aim of our approach is the computation of the ordinates b_k (and possibly the slopes s_k) of the piecewise approximation of $g_s(q(t))$ and not only the fitting of Equations (14) to experimental data. We also seek a description of the underlying linear dynamics of the structure through the estimation of $B(\omega)$ or its inverse, the frequency response function (FRF) matrix $H(\omega) = B^{-1}(\omega)$. To that purpose, we strictly follow the idea of the reference [9]. In brief, an invariant combination (with respect to a similarity transformation) of the estimated state matrices is built (termed extended frequency response function) from which the coefficient b_k (and possibly s_k) and the FRFs can be easily extracted.

The flowchart presented below summarises the FNSI methodology.

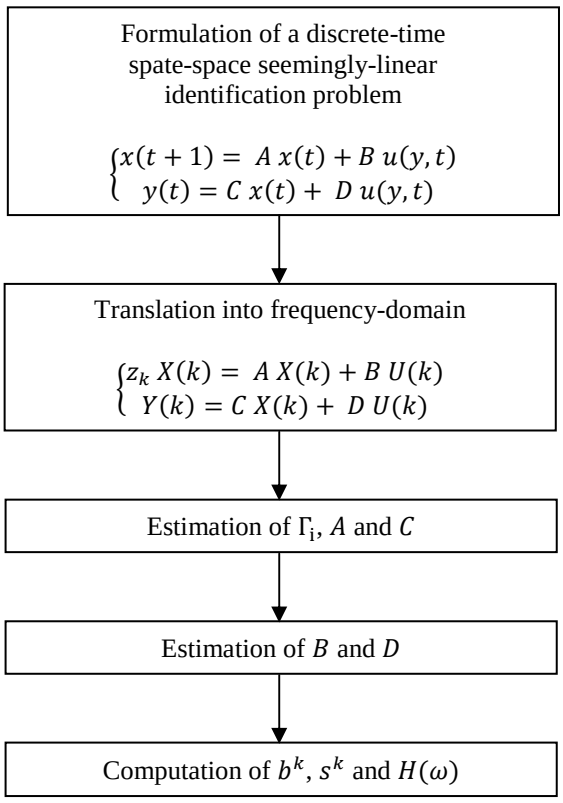

4. Numerical examples

Prior to addressing the identification of an experimental set-up in Section 5, we demonstrate the FNSI method based on a low-order local modelling of nonlinearities on numerical data. In particular, a comparison between the uses of first- and third-order piecewise polynomials is envisaged, both in terms of accuracy and efficiency. Two simple discrete structures are considered for this purpose, namely a Duffing oscillator and a five-DOF structure comprising two nonlinearities taken from [10].

4.1. Duffing oscillator

The vibrations of a Duffing oscillator are governed by the equation

$$M\,\ddot{q}(t) + C\,\dot{q}(t) + K\,q(t) + \mu\,q^3(t) = p(t). \tag{25}$$

The linear and nonlinear parameters selected in this analysis are listed in Table 1. The system was simulated using a nonlinear Newmark time integration scheme, considering a sampling frequency of 2,500 *Hz*. The excitation $p(t)$ was a periodic noise (a formal definition of a periodic noise can be found in [5], p. 73), consisting of a single band-limited (0 – 100 *Hz*) normally-distributed random signal (12,500 points) repeated 40 times. Its root-mean-square (RMS) value was set to 100 *N* and, as a general practice, transients were removed before processing data.

Table 1. Parameters of the Duffing oscillator.

M (*kg*)	C (*Ns/m*)	K (*kN/m*)	μ (*MN/m³*)
2	5	100	10
Damped frequency ω_d (*Hz*)		Damping percentage ε (%)	
35.59		0.56	

Only 17,100 out of 450,000 frequency lines spanning from 5 to 100 *Hz* were exploited in the inverse problem. Low-frequency and out-of-input-band components were thus rejected since the information content they convey is less valuable (except possibly for harmonic regions). In comparison with a time-domain identification scheme, the full time series would be processed leading to an increased computational burden. Figure 1 shows the reconstruction of the cubic stiffness curve $\mu\,q^3(t)$ using a piecewise linear model. Visually, the result is excellent and the errors made on the estimated linear properties ω_d and ε in Table 2 confirm the quality of the identification. Note that the displacement domain over which the restoring force is defined was divided into 8 sub-intervals of equal width, yielding 9 nonlinearities in input of the FNSI algorithm.

The recourse to a third-order local approximation of the nonlinearity improves the identification, as depicted in Figure 2. Higher-order piecewise approximations offer an appealing trade-off between the degree of approximation and the required refinement of the displacement grid. In Figure 2, 3 sub-intervals with equal length are considered, entailing 8 nonlinearities in input. The resulting errors on the linear properties are excellent and the time needed to inverse the model is similar to the piecewise linear case (see Table 2). Note that the number of sub-intervals in both cases was chosen such that comparable accuracy and efficiency were obtained. This proves that first-order continuity can be attained without requiring additional computational efforts.

Table 2. Number of intervals and of nonlinearities, errors on the linear parameters and computational time for linear and third-order spline-based modellings.

	Piecewise linear modelling	Piecewise third-order modelling
Number of intervals	8	3
Number of nonlinearities	9	8
Error on ω_d (%)	0.56	-0.32
Error on ε (%)	-0.10	0.54
Time (*s*)	3.74	3.13

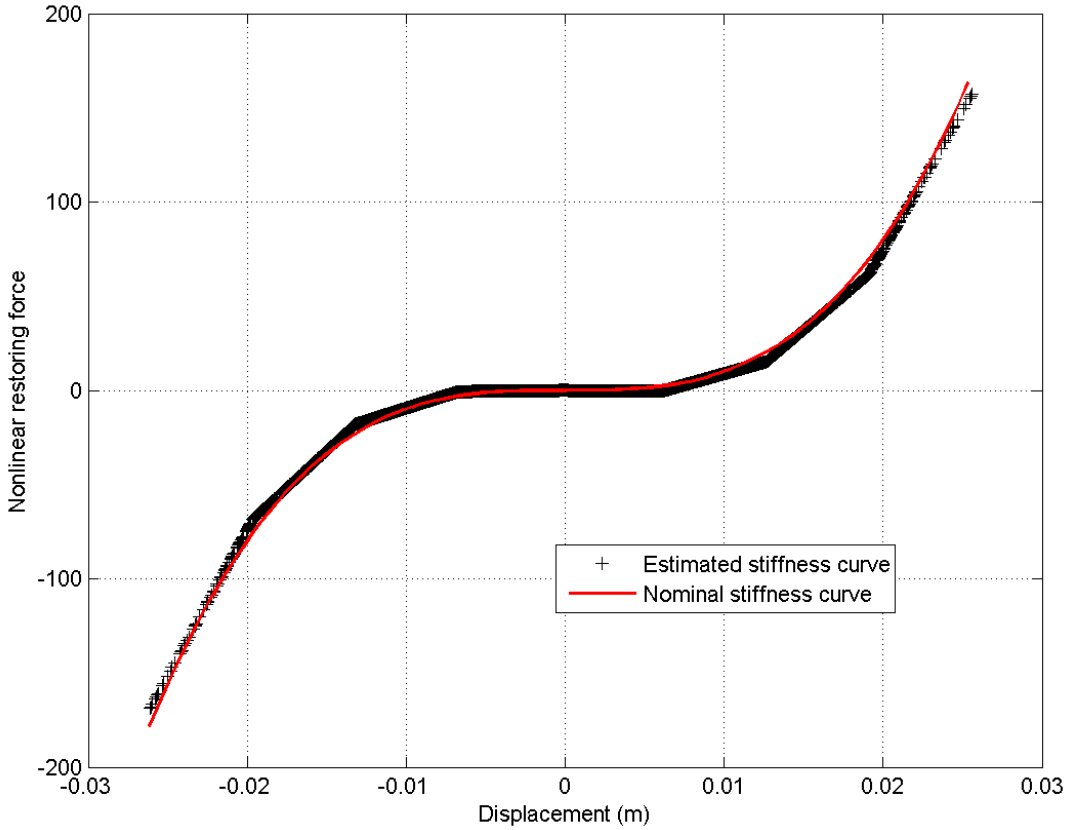

Figure 1. Duffing oscillator: piecewise linear estimation and nominal cubic stiffness curve.

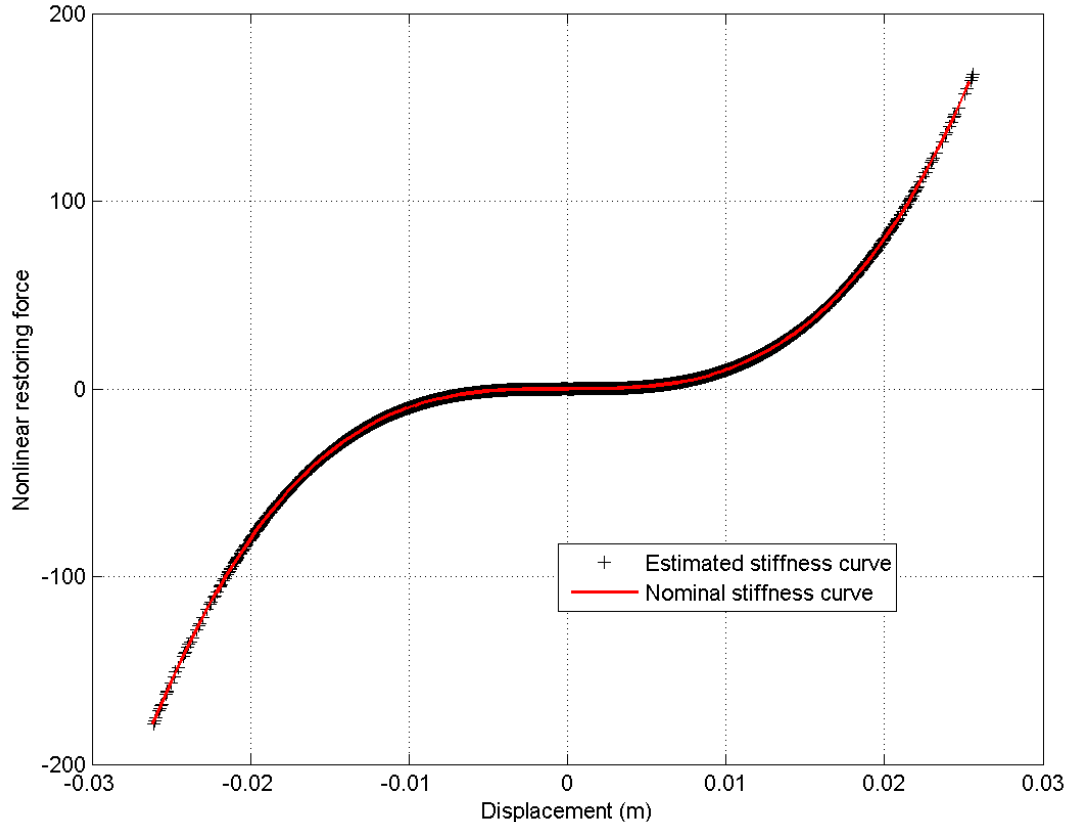

Figure 2. Duffing oscillator: piecewise third-order estimation and nominal cubic stiffness curve.

4.2. Multi-degree-of-freedom system with two nonlinearities

We now study the five-DOF structure in vertical translation depicted in Figure 3. The masses and linear dampers are all equal to 1 *kg* and 10 *Ns/m*, respectively. The linear springs possess stiffnesses of 50 *kN* except k_6 chosen equal to 35 *kN*. A cubic and an asymmetric quadratic-fifth order nonlinear springs connect m_2 and m_3 and m_3 and m_5, respectively. Their parameters are given in Table 3. A Newmark time integration scheme was used again sampling the signals at 5,000 *Hz*. A periodic noise forcing $p(t)$ was vertically applied to m_4 considering a RMS value of 500 *N*. It consisted of a single band-limited (0 – 100 *Hz*) normally-distributed random signal (10,000 points) repeated 40 times.

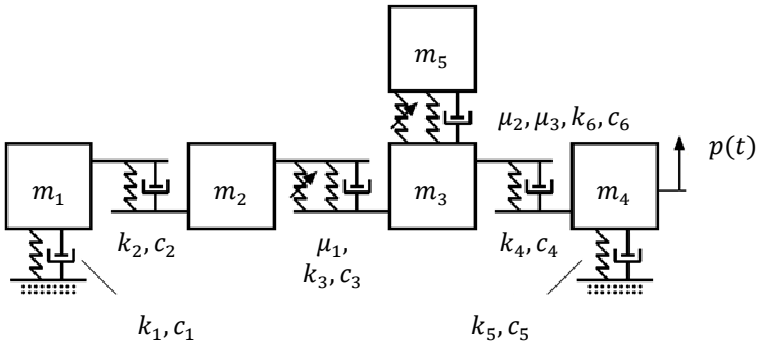

Figure 3. Schematic view of the multi-degree-of-freedom example.

Table 3. Nonlinear parameters of the five-DOF structure.

Location	Exponent	Stiffness parameter
2 – 3	3	500 (MN/m^3)
3 – 5	2	-500 (kN/m^2)
3 – 5	5	10 (GN/m^5)

Table 4. Number of intervals and of nonlinearities, errors on the linear parameters and computational time for linear and third-order spline-based modellings.

	Piecewise linear modelling	Piecewise third-order modelling
Number of intervals per nonlinearity	8	3
Number of nonlinearities	18	16
Error on ω_d (%)	[0.84 ; 2.68 ; 5.91 ; 0.17 ; 3.56]	[-1.09 ; -2.54 ; 1.56 ; -0.28 ; 4.59]
Error on ε (%)	[-2.14 ; -14.04 ; -27.85 ; 0.97 ; -81.97]	[5.23 ; 6.21 ; -4.50 ; 0.33 ; -10.68]
MAC values	[1.00 ; 0.96 ; 1.00 ; 0.99 ; 0.98]	[1.00 ; 0.98 ; 0.99 ; 0.99 ; 0.99]
Time (*s*)	66.92	51.65

We first consider approximations of the two nonlinearities using piecewise linear functions in Figures 4 and 5, where input and output spectra are processed between 5 and 100 *Hz*. The two fitted curves are found to have the necessary flexibility to cover a large variety of functional forms and to capture the complicated nature of stiffness in the system. In particular, a highly asymmetric behaviour of restoring force is correctly retrieved in Figure 5. Table 4 lists the errors made on the estimated linear properties of the system, *i.e.* the damped frequencies, damping ratios and Modal Assurance Criterion (MAC) values. The different visual and numerical quality indicators show that a linear spline-based approach, though suffering from some limitations, is a reliable tool for understanding nonlinear mechanisms.

Utilising third-order splines improves the accuracy of the identification, as already underlined in Section 4.1. and confirmed in Figures 6 and 7 and in Table 4. We opted for the same division of the displacement domains as in the Duffing example (see Table 4) to demonstrate again that a comparable numerical effort leads to enhanced results in the case of cubic approximations. Note that this does not necessarily imply that they should always be preferred over linear splines, *e.g.* in the case of first-order discontinuous nonlinearities.

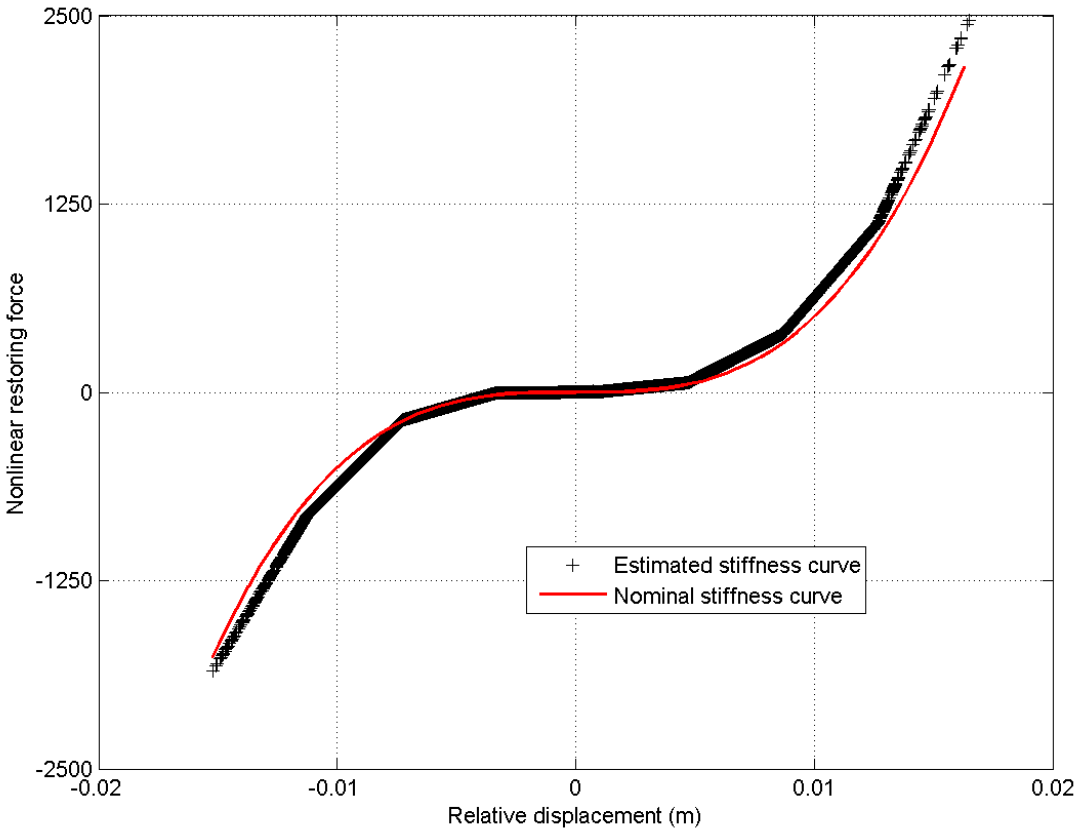

Figure 4. 5-DOF structure: piecewise linear estimation and nominal cubic stiffness curve.

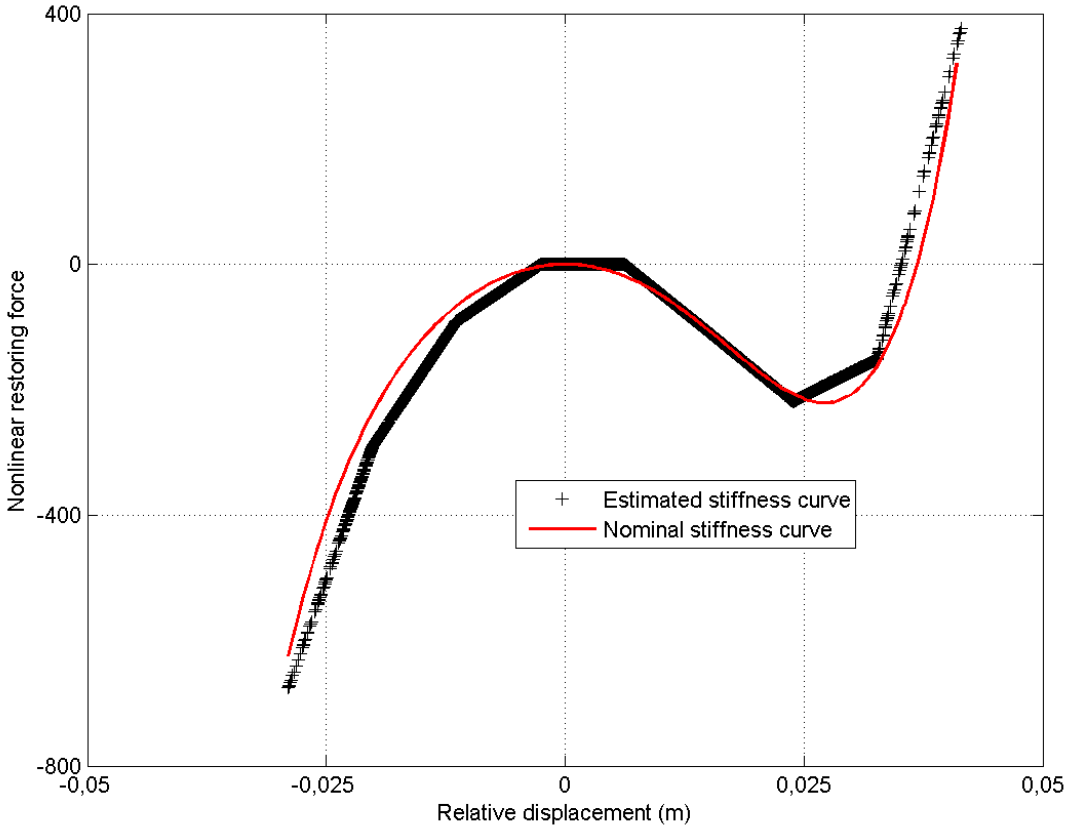

Figure 5. 5DOF-structure: piecewise linear estimation and nominal quadratic-fifth order stiffness curve.

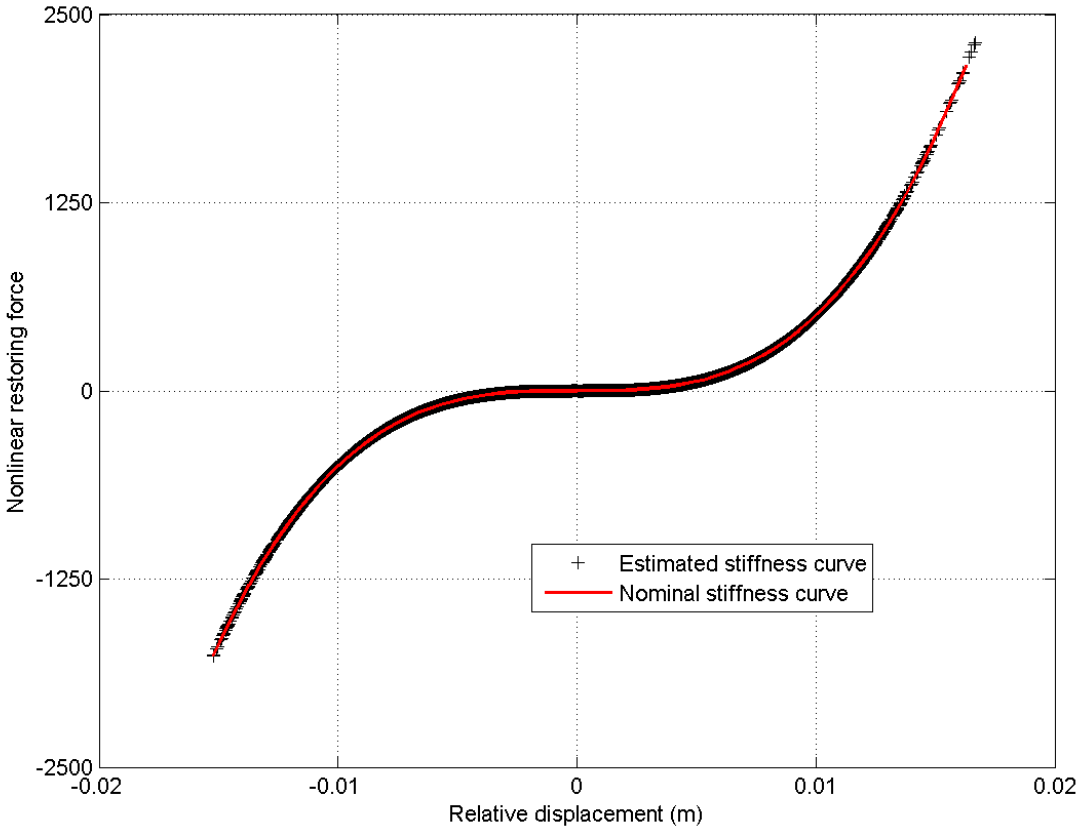

Figure 6. 5-DOF structure: piecewise third-order estimation and nominal cubic stiffness curve.

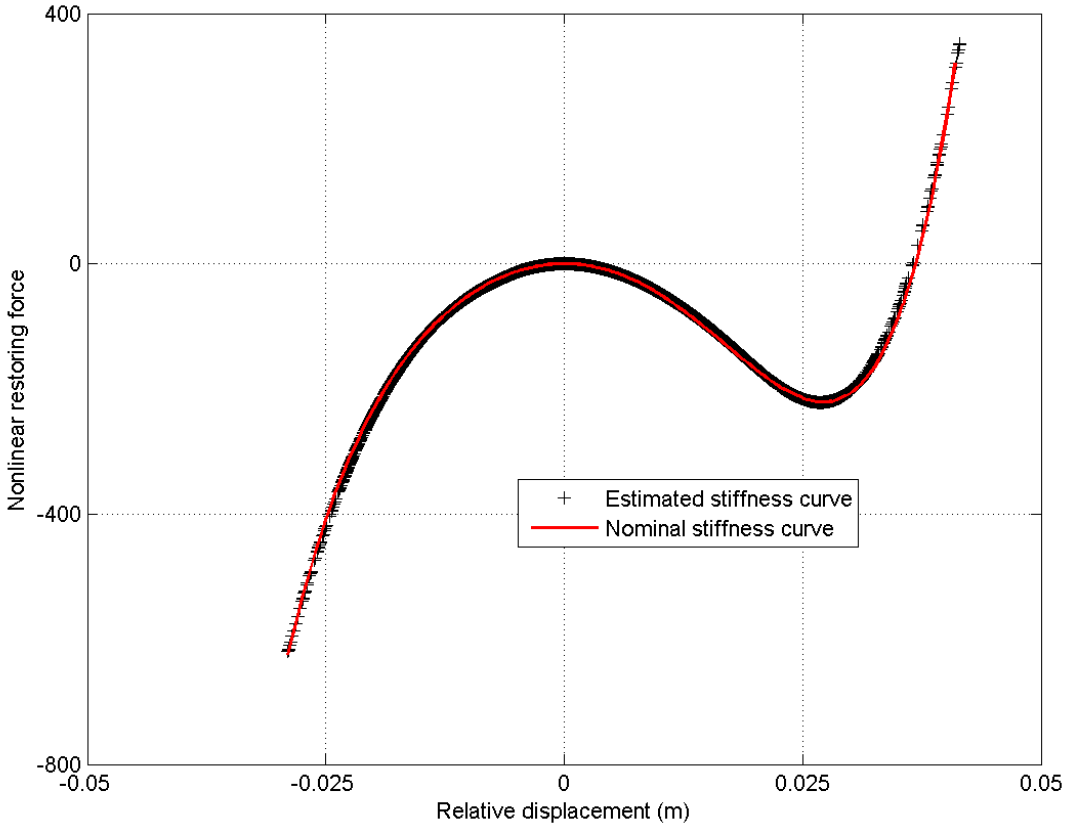

Figure 7. 5DOF-structure: piecewise third-order estimation and nominal quadratic-fifth order stiffness curve.

5. Experimental identification of a nonlinear beam

The benchmark involves a cantilever beam whose free end exhibits nonlinear geometrical behaviour because of an appended thin beam. The geometrical properties of the set-up are listed in Table 5. Seven accelerometers regularly spanned the main beam and an additional displacement sensor was positioned at its end. The thin part was mounted vertically (see Figure 8) to limit the effect of gravity. The excitation force was a band-limited (0 – 500 *Hz*) white-noise sequence sampled at 2,560 *Hz* and applied in a horizontal plane by a shaker located 30 *cm* away from the clamping. Seven excitation levels were considered from 0.56 *N* RMS up to 27.73 *N* RMS and 163,840 time samples were recorded for each. The first fifth of those samples was rejected to limit the effect of transients on the identification.

Table 5. Geometrical properties of the nonlinear beam set-up.

	Length (*m*)	Width (*mm*)	Thickness (*mm*)
Main beam	0.7	14	14
Thin beam	0.04	14	0.5

At the lowest excitation level (0.56 *N* RMS), the structure is known to behave linearly [11]. A FNSI analysis allows to extract its linear damped frequencies, damping ratios and mode shapes. Figure 9 shows how closely the identified FRF at beam tip matches the linear H2 estimation. The 3 first bending modes of the beam are identified in the 0 – 500 *Hz* range corresponding to frequencies of 30.71 *Hz*, 139.49 *Hz* and 390.33 *Hz*, respectively. Damping ratios are estimated at 0.345 %, 0.093 % and 0.081 %, respectively.

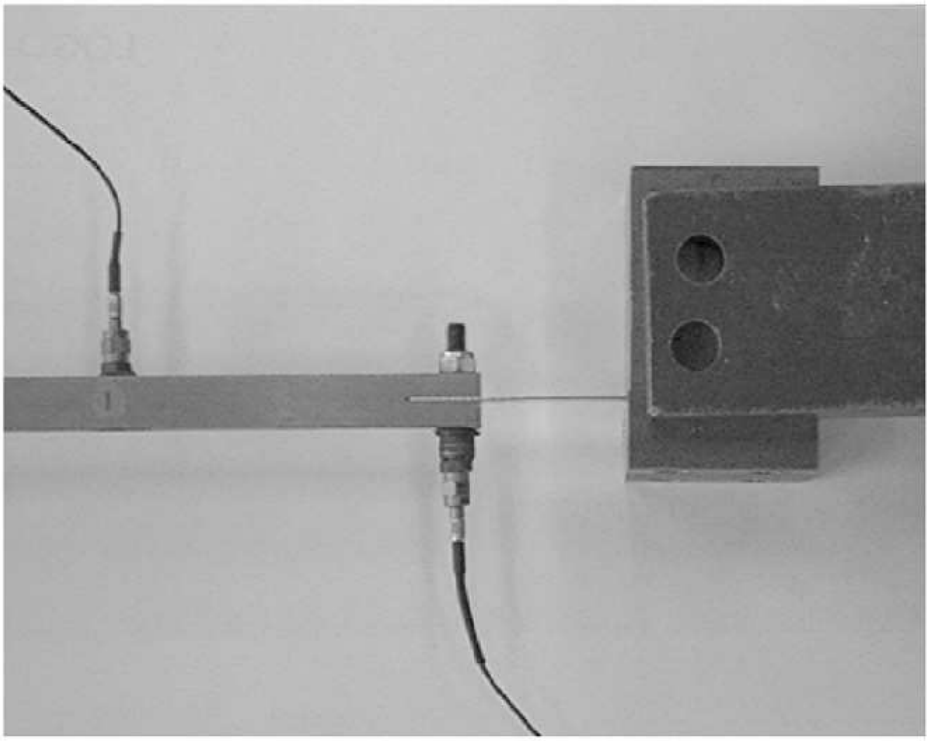

Figure 8. Top view of the nonlinear beam set-up where the thin beam is mounted vertically.

We consider the highest level of excitation at 27.73 *N* RMS and process frequencies in the neighbourhood of the 3 resonances only (25 – 35, 135 – 145 and 385 – 395 *Hz*). Figures 10 and 11 show the reconstruction of the nonlinear restoring force curve at beam tip and describe how the thin beam stiffens the structure. Both approximations are compared with a reference curve which considers a global modelling of the form $g(q) = \mu\,|q|^{\alpha}\,\mathrm{sign}(q)$, where α = 2.8 and μ = 2.2 10^9 $N/m^{2.8}$. This estimation was carried out in [11] using the conditioned reverse path (CRP) method [10]. The piecewise linear and third-order results are found to be meaningful and in accordance with the global polynomial. A slight discrepancy is observed in negative relative displacement where the spline-based modelling reveals a softer behaviour than the CRP estimation. This assymetry might be attributed to gravity which induced a prestress in the thin beam.

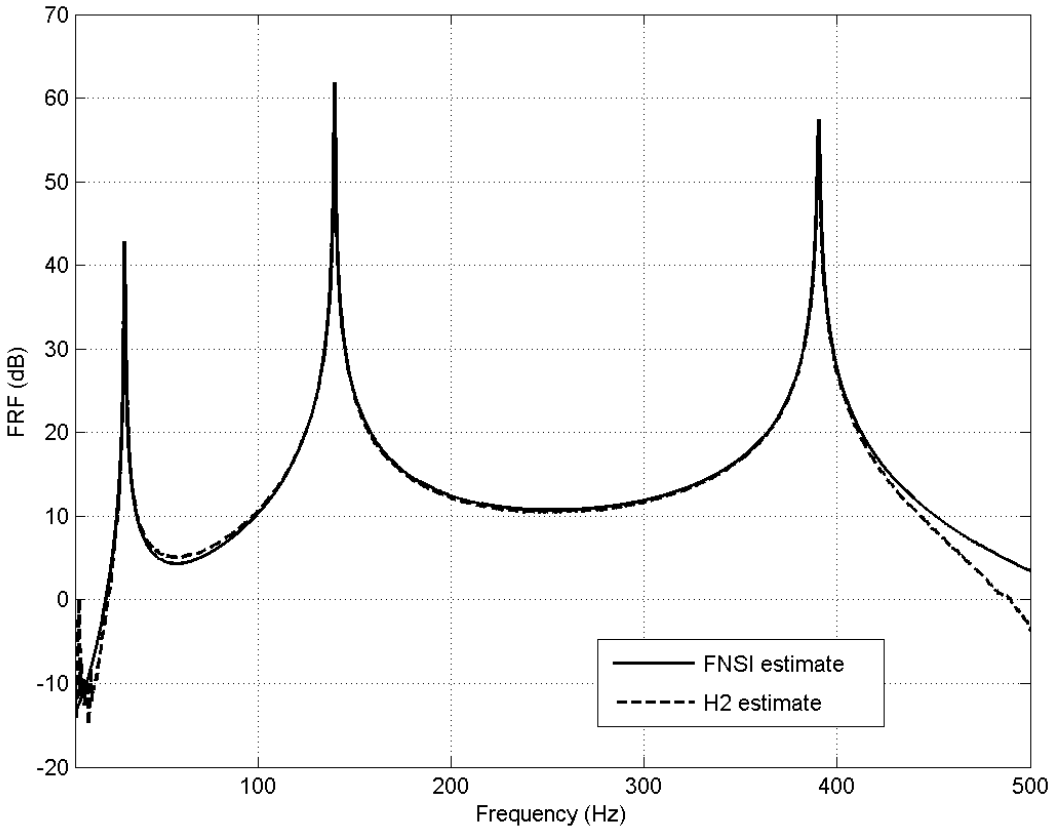

Figure 9. FRF at beam tip at low level using the FNSI method and non-parametric H2 estimate.

The analysis of the results listed in Table 6 shows that the low-level linear properties of the structure (damped frequencies and mode shapes) are correctly estimated from nonlinear data. As in the numerical cases, enforcing first-order continuity improves the result without reducing the computational efficiency. Note that the deviations observed on the damping ratios from low-level data are not reported herein because of the possible nonlinear nature of damping in the structure which would bias the comparison.

Table 6. Number of intervals and of nonlinearities, errors on the linear parameters and computational time for linear and third-order spline-based modellings.

	Piecewise linear modelling	Piecewise third-order modelling
Number of intervals	8	3
Number of nonlinearities	9	8
Deviation on ω_d (%)	[1.41 ; 1.12 ; 0.51]	[0.77 ; 1.29 ; 0.47]
MAC values	[0.97 ; 1.00 ; 1.00]	[0.98 ; 1.00 ; 1.00]
Time (s)	12.52	10.51

6. Conclusions

Characterisation of structural nonlinearities, *i.e.* the determination of an adequate model form, is known to be of utmost importance in view of system identification. In this context, the present paper aimed at introducing a low-order local modelling strategy within the framework of the Frequency-domain Nonlinear Subspace Identification (FNSI) method. Piecewise linear and third-order polynomial-based approaches were applied to two academic structures and then to the experimental identification of a nonlinear beam. They both proved to yield a reliable modelling of the involved nonlinear mechanisms. Finally, first-order continuity offered by cubic splines was shown to improve the accuracy of the identification without comprising its efficiency.

Further work should focus on the robustness assessment of this low-order local modelling of nonlinearities. In particular, it is known that a nonlinear restoring force computed through the FNSI method should be zero and have zero slope at equilibrium. It should therefore be valuable to enforce *a priori* these two constraints while this work only considers an *a posteriori* correction. An automatic selection of the number of sub-intervals or iterative approximations considering an adaptative refinement strategy would be other advances.

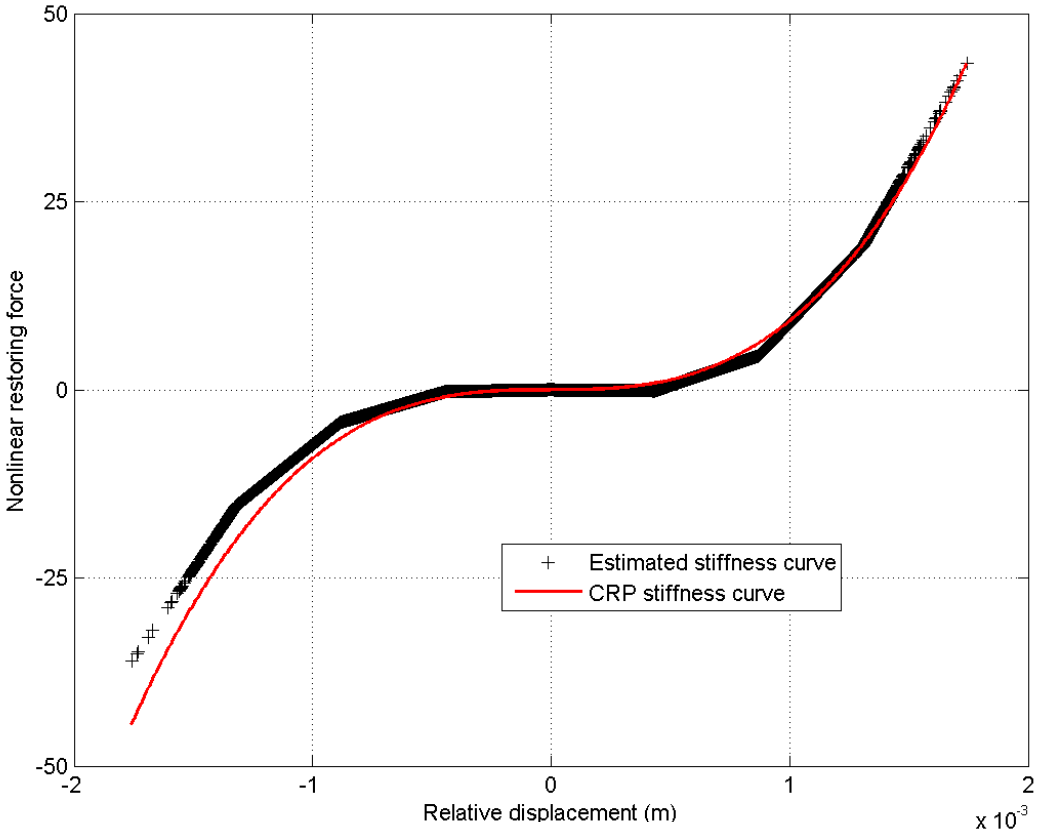

Figure 10. Nonlinear beam: piecewise linear estimation and CRP stiffness curve.

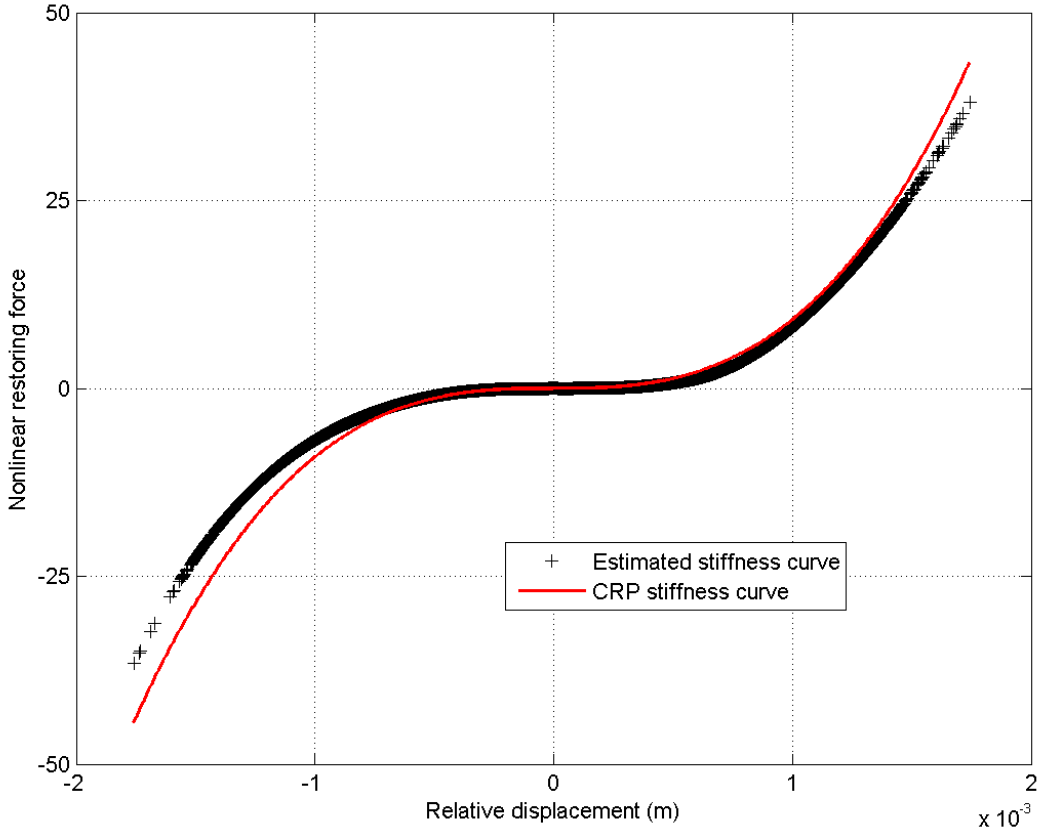

Figure 11. Nonlinear beam: piecewise third-order estimation and CRP stiffness curve.

Acknowledgement

The author J.P. Noël would like to acknowledge the Belgian National Fund for Scientific Research (FRIA fellowship) for its financial support.

References

1. G. Kerschen, K. Worden, A. F. Vakakis and J.C. Golinval, *Past, present and future of nonlinear system identification in structural dynamics.* Mechanical Systems and Signal Processing, 2006. **20**, 505-592.

2. S. F. Masri and T. K. Caughey, *A nonparametric identification technique for nonlinear dynamic problems.* Journal of Applied Mechanics, 1979. **46**, 433-447.

3. S. L. Lacy and D. S. Berstein, *Subspace identification for non-linear systems with measured-input non-linearities.* International Journal of Control, 2005. **78**, 906-926.

4. P. Van Overschee and B. De Moor, *Continuous-time frequency domain subspace system identification.* Signal Processing, 1996. **52**, 179-194.

5. R. Pintelon and J. Schoukens, *System Identification: A Frequency Domain Approach.* IEEE Press, Piscataway, 1998.

6. R. Pintelon, *Frequency-domain subspace system identification using non-parametric noise models.* Automatica, 2002. **38**, 1295-1311.

7. P. Van Overschee and B. De Moor, *Subspace Identification for Linear Systems.* Kluwer Academic Publishers, Boston/London/Dordrecht, 1996.

8. T. McKelvey, H. Akçay and L. Ljung, *Subspace-based multivariable system identification from frequency response data.* IEEE Transactions on Automatic Control, 1996. **41**, 960-979.

9. S. Marchesiello and L. Garibaldi, *A time domain approach for identifying nonlinear vibrating structures by subspace methods.* Mechanical Systems and Signal Processing, 2008. **22**, 81-101.

10. C. M. Richards and R. Singh, *Identification of multi-degree-of-freedom non-linear systems under random excitations by the "reverse path" spectral method.* Journal of Sound and Vibration, 1998. **213**(4), 673-708.

11. G. Kerschen, V. Lenaerts and J.C. Golinval, *Identification of a continuous structure with a geometrical non-linearity. Part I: Conditioned reverse path method.* Journal of Sound and Vibration, 2003. 262, 8.